

## Chapter 4 (2.1) Flow Past Cylinders and Spheres

### Flow Past Cylinders and Spheres

Low  $Re = \rho U \infty / \mu < 1$

No slip  $\Rightarrow$  velocity  $\Rightarrow$  diffusion (not convection) away from surface.

Oseen: laminar as per Stokes results  
convection results in free/ft symmetry  
free/ft asymmetry but  
neg marginal moment  $C_D = \frac{24}{Re} (1 + \frac{3}{16} Re)$

$Re > 1$  Oseen breakdown of velocity  
massive confined behind cylinder/sphere

$Re > 4$  two eddies form closed separation  
Subtle behind cylinder. Kármán wake.

Modest  $Re$   $Re > 40$  wake unstable at  
when reaches  $10^2$  wake oscillates with  
 $\approx$  periodic in time at downstream distance,  
i.e., Kármán vortex street: staggered rows  
of vortices with opposite rotation. von Kármán  
studied as superposition unsteady vortices  
& showed staggered vs non-staggered stable  
if the ratio  $\Delta y / \Delta x = 0.28$ . Vortices move  
downstream at speed less  $U$ , which means  
slowly follow cylinder.

$40 < Re < 80$  separation subtle & vortex street  
do not interact.  $L_{SS}$  increases.

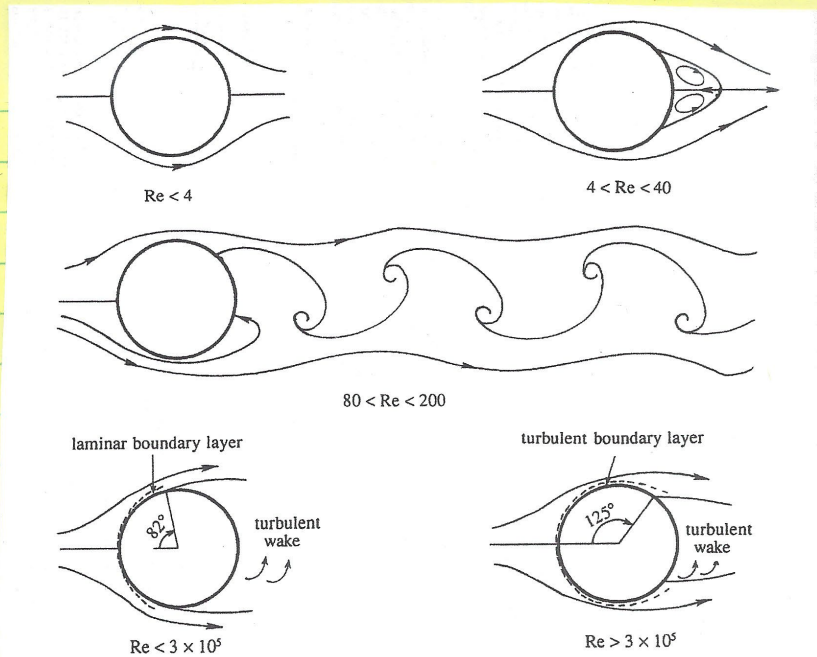


FIGURE 10.18 Depiction of some of the flow regimes for a circular cylinder in a steady uniform cross flow. Here,  $Re = U_\infty d / \nu$  is the Reynolds number based on free-stream speed  $U_\infty$  and cylinder diameter  $d$ . At the lowest  $Re$ , the streamlines approach perfect fore-aft symmetry. As  $Re$  increases, asymmetry increases and steady wake vortices form. With further increase in  $Re$ , the wake becomes unsteady and forms the alternating-vortex von Karman vortex street. For  $Re$  up to  $Re_{cr} \sim 3 \times 10^5$ , the laminar boundary layer separates approximately  $82^\circ$  from the forward separation point. Above this  $Re$  value, the boundary-layer transitions to turbulence, and separation is delayed to  $125^\circ$  from the forward separation point.

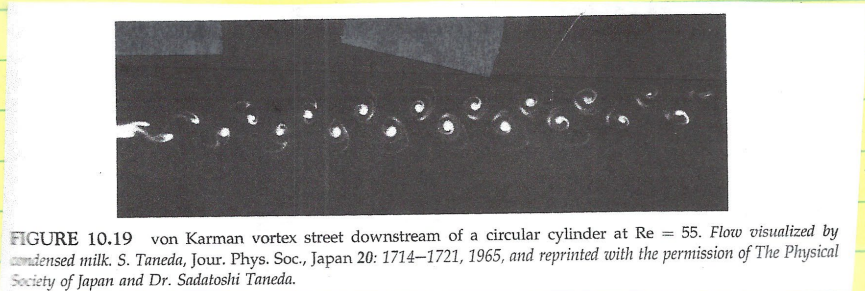


FIGURE 10.19 von Karman vortex street downstream of a circular cylinder at  $Re = 55$ . Flow visualized by condensed milk. S. Taneda, Jour. Phys. Soc., Japan 20: 1714–1721, 1965, and reprinted with the permission of The Physical Society of Japan and Dr. Sadatoshi Taneda.

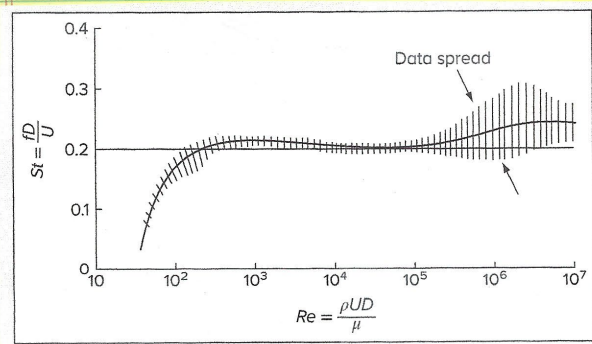
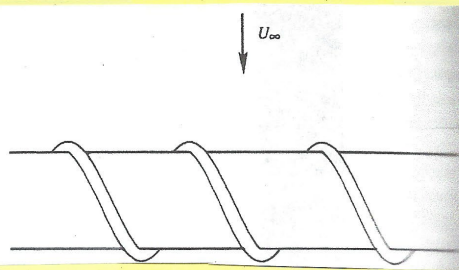


FIGURE 1-7 Measured Strouhal number for vortex shedding frequency behind a circular cylinder.

$Re > 80$   $Re$  increases  $\sim 20$  it becomes unstable  
 a vorticity or vortex sheet moves closer  
 cylinder. Attached eddies shed periodically  
 from each side cylinder alternately  
 result in alternating circulation of side  
 force to flow direction  $U_{\infty}$  at Strouhal  
 number  $St = \omega d / U_{\infty}$ .

FIGURE 10.20 Spiral blades used for  
 breaking up the span-wise coherence of vortex  
 shedding from a cylindrical rod. Coherent vortex  
 shedding can produce tonal noise and potentially  
 large (and undesired) structural loads on engi-  
 neered devices that encounter wind or water  
 currents.



For small  $d$  moderate  $U_{\infty}$   $St$  in  
 acoustic range:  $U_{\infty} = 10 \text{ m/s}$   $d = 2 \text{ mm}$   
 $St = 0.2 \Rightarrow f = 1000 \text{ cycles/s} \Rightarrow \text{Singing}$

$Re < 200$  wake vortices laminar for  
 long distance

$Re > 200$  vortex sheet unstable, irregular,  
 or chaotic flow between the vortices.

At  $Re > 3000$   $St$  only evident near  
 cylinder or wake fully turbulent  
 for  $x > 3D$

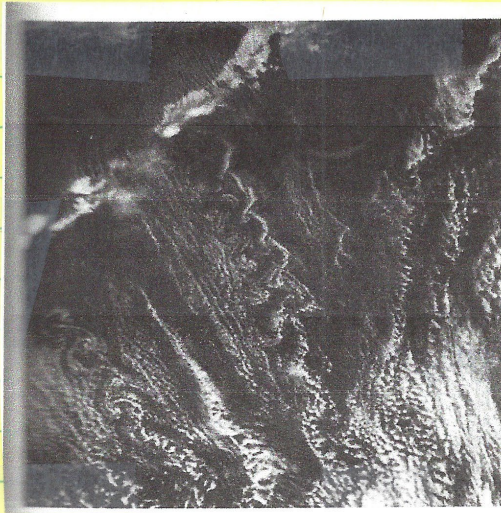


FIGURE 10.21 A von Karman vortex street downstream of mountain peaks in a strongly stratified atmosphere. There are several mountain peaks along the linear, light-colored feature running diagonally in the upper-left quadrant of the photograph. North is upward, and the wind is blowing toward the southeast. R. E. Thomson and J. F. R. Gower, *Monthly Weather Review* 105: 873-884, 1977; reprinted with the permission of the American Meteorological Society.

Figure

$Re < 3 \times 10^5 = 300,000$  : laminar BL,  $\theta_s \approx 82^\circ$ ,  
 base pressure  $\sim$  constant  $<$  free stream pressure.  
 $C_D$  due  $C_{Dp} \gg C_{Df}$  since  $\theta_s \sim$  constant  
 $C_D \sim$  constant up to  $Re_{cr} \approx 3 \times 10^5 = f(\text{free stream KE \& roughness})$

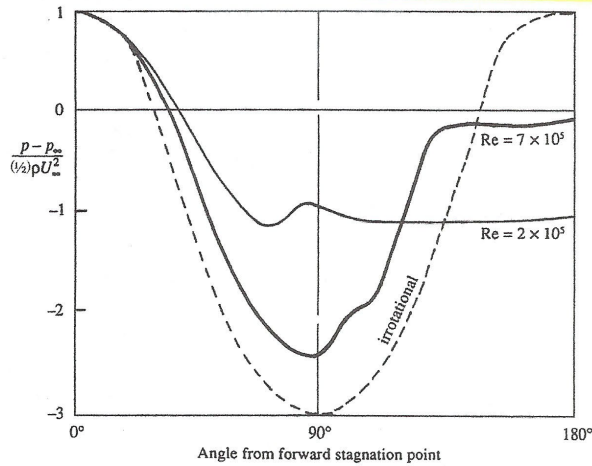


FIGURE 10.22 Surface pressure distribution around a circular cylinder at subcritical and supercritical  $Re$  numbers. Note that the pressure is nearly constant within the wake and that the wake is narrower for supercritical  $Re$ . The change in the top- and bottom-side, boundary-layer separation points near  $Re_{cr}$  is responsible for the change in  $C_D$  shown.

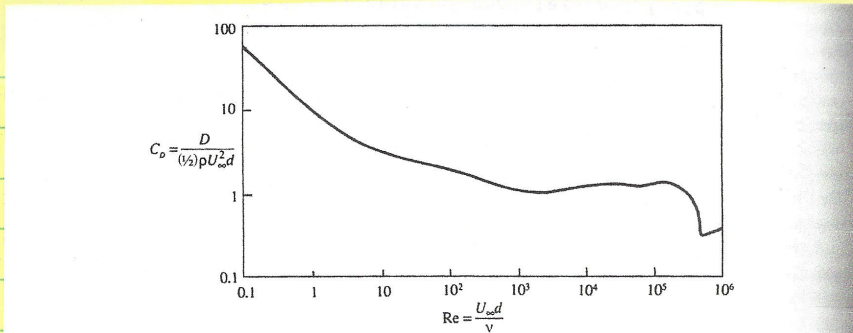


FIGURE 10.23 Measured drag coefficient,  $C_D$ , of a smooth circular cylinder vs.  $Re = U_\infty d/\nu$ . The sharp dip near  $Re_{cr}$  is due to the transition of the boundary layer to turbulence, and the consequent downstream movement of the point of separation and change in the cylinder's surface pressure distribution.

$3 \times 10^5 < Re < 3 \times 10^6$  laminar BL transition  
 further BL which is resistant separation  
 such that  $\theta_s \approx 125^\circ \Rightarrow$  thinner wake,  
 reduced  $C_D$  i.e. drag crisis with  
 $C_p$  closer potential flow.  $C_D$  drops from 1.2  
 to 0.33 at  $Re_{crit}$   
 $Re > 3 \times 10^6$   $\theta_s$  reduces somewhat &  $C_D$  increases

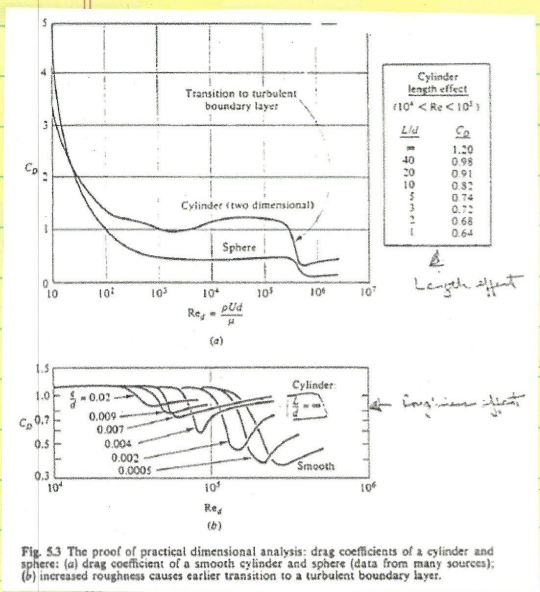


Fig. 5.3 The proof of practical dimensional analysis: drag coefficients of a cylinder and sphere: (a) drag coefficient of a smooth cylinder and sphere (data from many sources); (b) increased roughness causes earlier transition to a turbulent boundary layer.

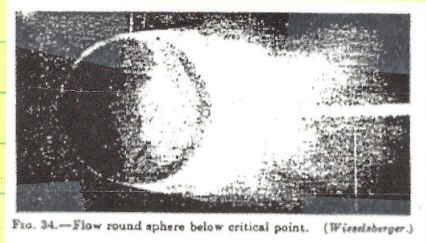


Fig. 34.—Flow round sphere below critical point. (Wieselsberger.)

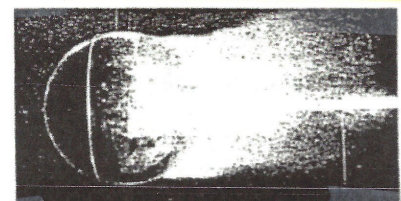


Fig. 35.—Owing to a thin wire ring round the sphere, the flow becomes of the other type with turbulent boundary layer. (Wieselsberger.)

Circular inviscid features:

$$1. Re = \frac{Ua}{\nu}$$

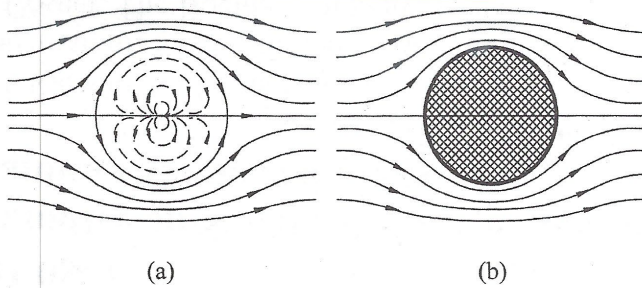


FIGURE 4.8 (a) Flow field represented by the complex potential  $F(z) = U(z + a^2/z)$  and (b) flow around a circular cylinder of radius  $a$ .

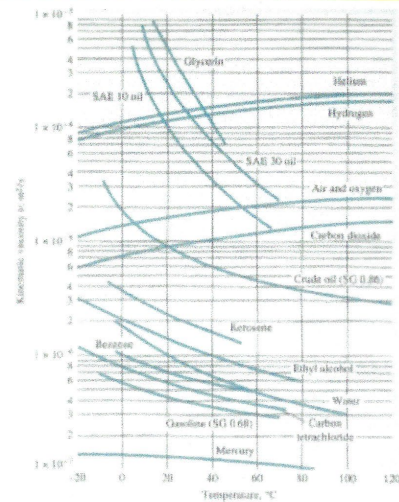


Table 4.2 Kinematic viscosity of common fluids at 1 atm.

Ideal or inviscid flow is even very small viscosity  $\neq 0$  has profound effects on flow due to viscosity, BL, and separation induces asymmetry of  $C_D$  or slip, symmetry, and d'Alembert paradox  $C_D = 0$ .

2. Symmetric geometry of BC can have asymmetric solutions
3. For range of  $Re$ , roughness, free stream TKE, etc. can reduce  $C_D$  due to separation control, i.e.,  $C_D$  increase of narrower wake for smooth surface separation e.g. cylinder and sphere

# VORTEX DYNAMICS IN THE CYLINDER WAKE

C. H. K. Williamson

Mechanical and Aerospace Engineering, Upson Hall, Cornell University,  
Ithaca, New York 14853

KEY WORDS: wakes, instability, vortex shedding

## ABSTRACT

Since the review of periodic flow phenomena by Berger & Wille (1972) in this journal, over twenty years ago, there has been a surge of activity regarding bluff body wakes. Many of the questions regarding wake vortex dynamics from the earlier review have now been answered in the literature, and perhaps an essential key to our new understandings (and indeed to new questions) has been the recent focus, over the past eight years, on the three-dimensional aspects of nominally two-dimensional wake flows. New techniques in experiment, using laser-induced fluorescence and PIV (Particle-Image-Velocimetry), are vigorously being applied to wakes, but interestingly, several of the new discoveries have come from careful use of classical methods. There is no question that strides forward in understanding of the wake problem are being made possible by ongoing three-dimensional direct numerical simulations, as well as by the surprisingly successful use of analytical modeling in these flows, and by secondary stability analyses. These new developments, and the discoveries of several new phenomena in wakes, are presented in this review.

*Annu. Rev. Fluid. Mech. 1996. 28:477–539*

Copyright © 1996 by Annual Reviews Inc. All rights reserved

Applied Ocean Research 59 (2016) 663–675



Contents lists available at ScienceDirect

Applied Ocean Research

Journal homepage: [www.elsevier.com/locate/apor](http://www.elsevier.com/locate/apor)



## Large-eddy simulation of the flow past a circular cylinder at sub- to super-critical Reynolds numbers



Seong Mo Yeon, Jianming Yang, Frederick Stern\*

*IHR-Hydroscience and Engineering University of Iowa, Iowa City, IA 52242, USA*

### ARTICLE INFO

Article history:  
Received 26 January 2015  
Received in revised form 5 October 2015  
Accepted 12 November 2015  
Available online 23 December 2015

Keywords:  
Large-eddy simulation  
Circular cylinder  
Critical Reynolds number  
Drag crisis  
Verification and validation

### ABSTRACT

Large-eddy simulation of turbulent flow past a circular cylinder at sub- to super-critical Reynolds numbers is performed using a high-fidelity orthogonal curvilinear grid solver. Verification studies investigate the effects of grid resolution, aspect ratio and convection scheme. Monotonic convergence is achieved in grid convergence studies. Validation studies use all available experimental benchmark data. Although the grids are relatively large and fine enough for sufficiently resolved turbulence near the cylinder, the grid uncertainties are large indicating the need for even finer grids. Large aspect ratio is required for sub-critical Reynolds number cases, whereas small aspect ratio is sufficient for critical and super-critical Reynolds number cases. All the experimental trends were predicted with reasonable accuracy, in consideration the large facility bias, age of most of the data, and differences between experimental and computational setup in particular free stream turbulence and roughness. The largest errors were for under prediction of turbulence separation.

© 2015 Elsevier Ltd. All rights reserved.

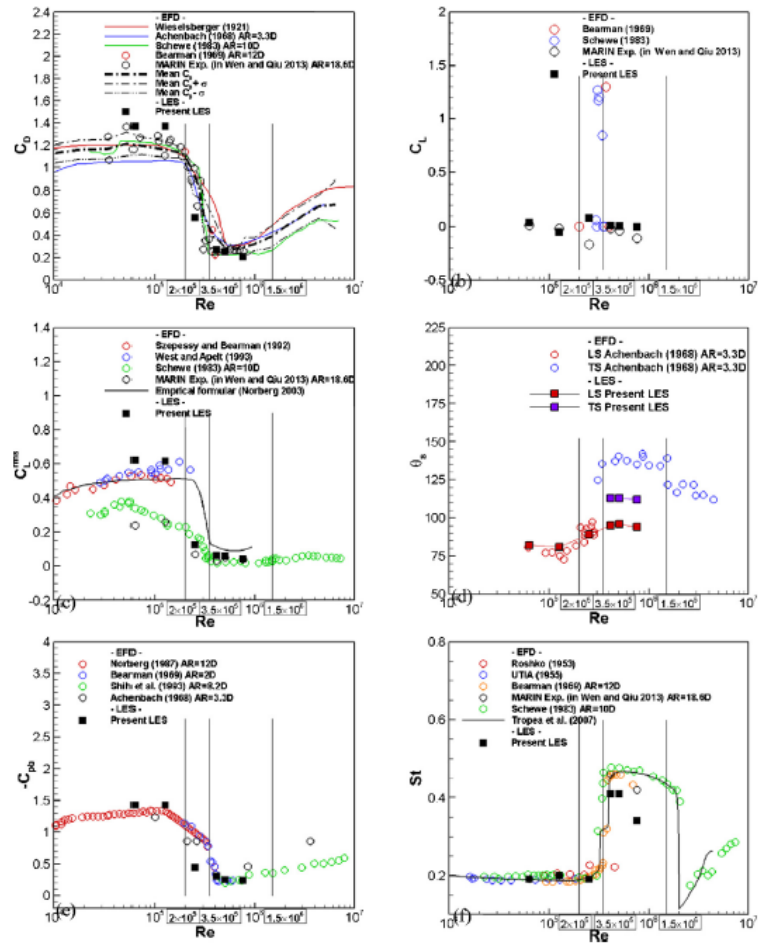


Fig. 2. Drag (a), lift (b), RMS lift (c) coefficients, separation angle (d), base pressure (e) and Strouhal number (f) as functions of Re.

672

S.M. Yeon et al. / Applied Ocean Research 59 (2016) 663–675

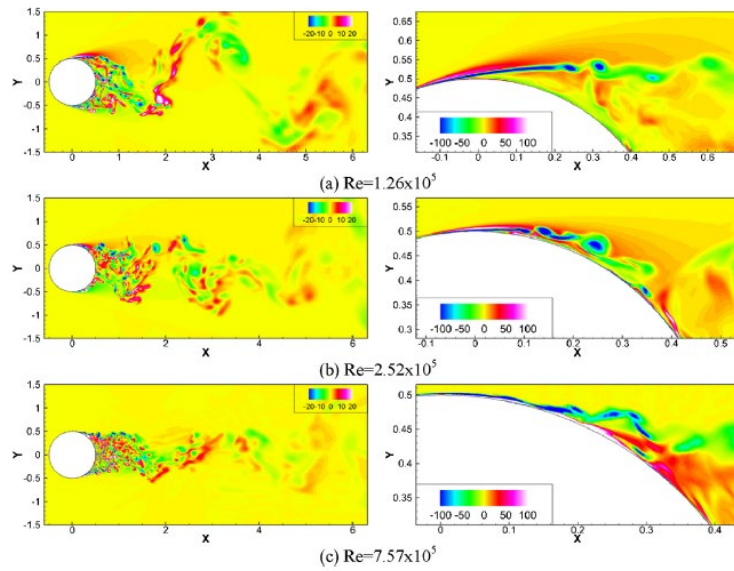
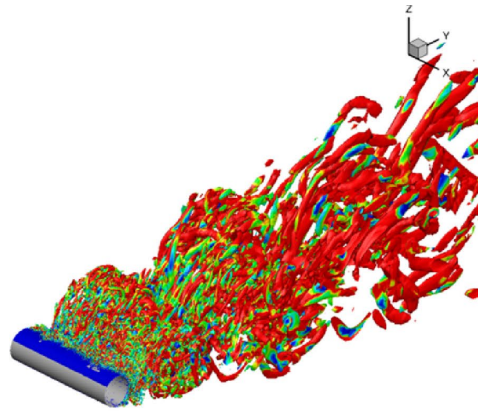
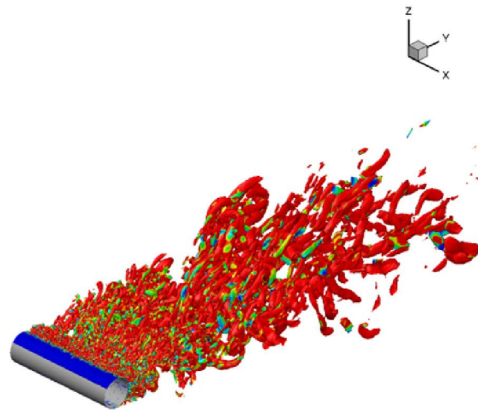


Fig. 7. Instantaneous spanwise vorticity contours, right side shows the close-up views.

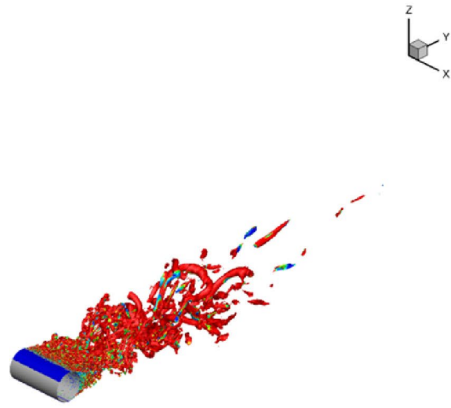




(a) sub-critical ( $Re=1.26 \times 10^5$ )



(b) critical ( $Re=2.52 \times 10^5$ )



(c) super-critical ( $Re=7.57 \times 10^5$ )

**Fig. 8.** Vortex structures with isosurfaces of Q-criterion colored by  $v_d/v$ .

## Integrated High-Fidelity Validation Experiments and LES for a Surface-Piercing Truncated Cylinder for Sub and Critical Reynolds and Froude Numbers

Frederick Stern

IHR-Hydrosience and Engineering University of Iowa  
Iowa City, IA 52242  
USA

frederick-stern@uiowa.edu

### ABSTRACT

*Integrated high-fidelity validation towing tank experiments and LES are presented for a surface-piercing truncated cylinder for sub- and critical Reynolds and Froude numbers, as a unit problem case study. The physics of interest are the effects of air-water interface on turbulence anisotropy and vortex shedding, 3D separation, transition to turbulence and the drag crisis; the effects of the truncated bottom; and ultimately bubble/droplet size distributions. The integrated experiments and LES was successful in using preliminary LES to guide the experiments especially for local flow surface pressure and flow field measurements. Experimental pacesetting issues were the difficulty of the PIV experiments; nonetheless, the data already collected is useful and valuable as the benchmark for LES validation. The largest hurdle in achieving the desired outcomes, however, was the LES since the current grid design and sizes required large computational resources. The experiments once completed will provide sufficient validation data for sub- and critical  $Re$  for many physics of interest. Experiments for spray droplet and air bubble size distribution measurements are still required. The LES at the current grid resolutions is able to fully-resolve the sub-critical but not the critical  $Re$  flow. Finer grids for critical  $Re$  are still required. Code development for overset grids, conservative convection schemes, and air/water interface LES models are also required. Future experiments and LES should focus on these issues along with extensions for VIV using towing tank PMM for pure sway motion.*

### NOMENCLATURE

AR	Aspect Ratio = $L/D$
$C_D$	Drag coefficient
$C_L$	Lift coefficient
$C_{LRMS}$	RMS lift coefficient
$C_d$	Sectional drag coefficient
$C_l$	Sectional lift coefficient
$C_p$	Pressure coefficient
$D$	Cylinder diameter
$E$	Comparison error = $(D-S)\%D$ where $D$ and $S$ are data and simulation values
$f_k$	Karman shedding frequency
$f_{sL}$	Shear layer frequency
Fr	Froude number = $U/(gD)^{1/2}$
$k$	Turbulent kinetic energy
$U_c$	Towing carriage speed

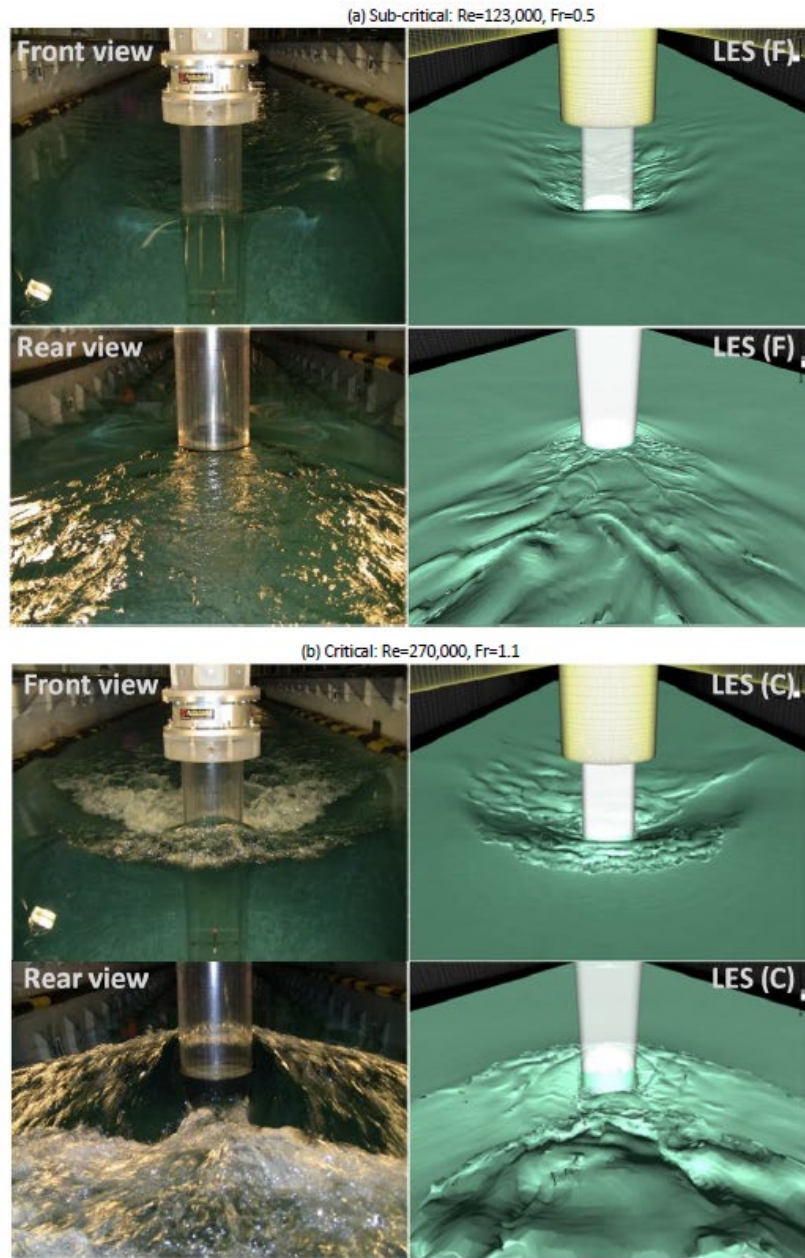


Figure 11-8: Photos of free surface waves around the cylinder model and comparisons with CFD simulations.

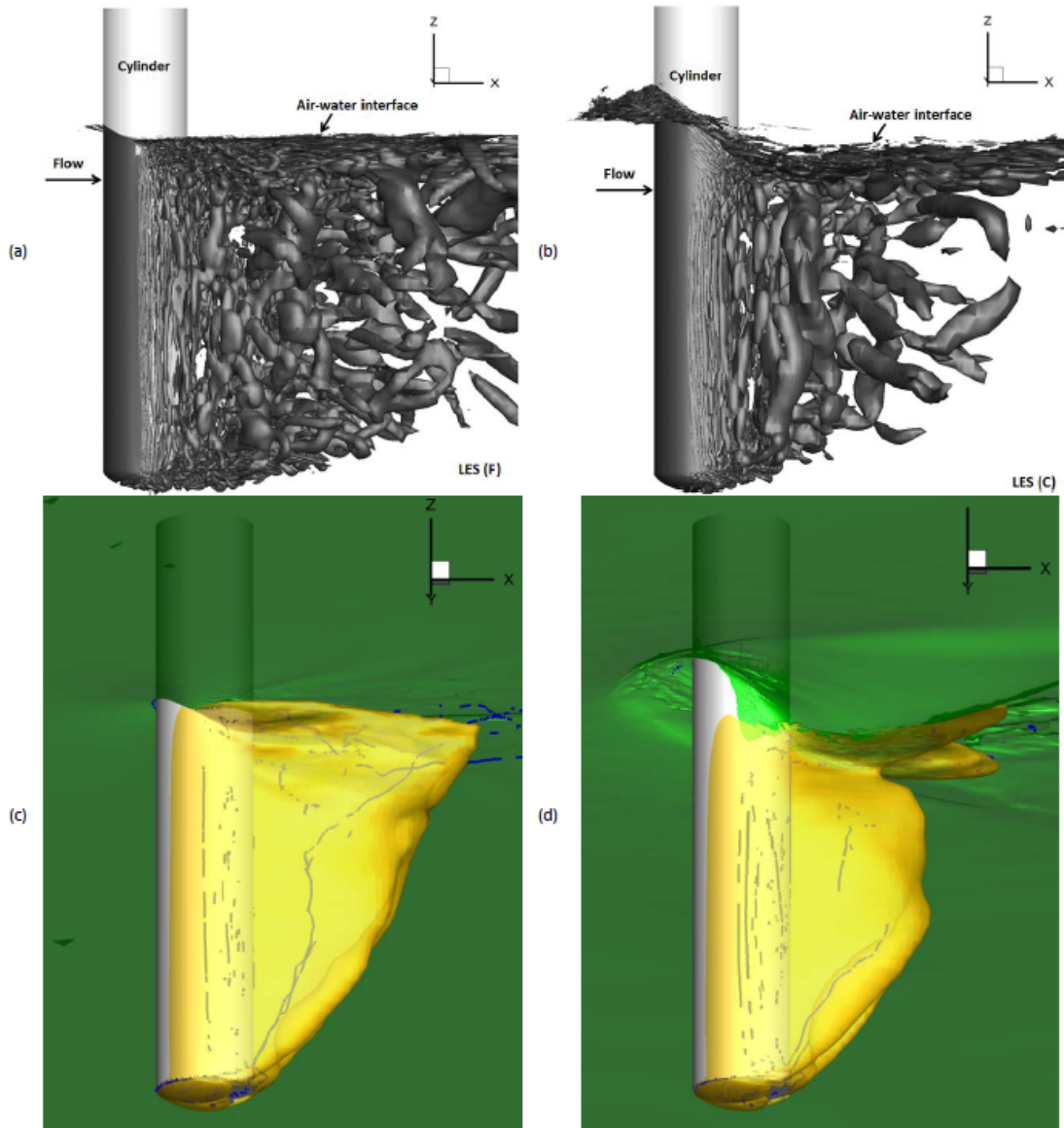


Figure 11-19: Iso-surface of instantaneous Q-criterion ( $Q=2$ ): (a) sub-critical Re, (b) critical Re; Mean flow separation pattern with vortex core line: visualized approximately using the iso-surfaces of the stagnation  $C_p=-0.3$ , (c) sub-critical Re, (d) critical Re.

## Effects of Sway Motion on Smooth-Surface Vortex Separation Onset and Progression: Surface Combatant and Surface-Piercing Truncated Cylinder

Frederick Stern

IIHR-Hydroscience and Engineering University of Iowa  
Iowa City, IA 52242  
USA

frederick-stern@uiowa.edu

### ABSTRACT

*The effects of sway motion on smooth-surface vortex separation onset and progression is studied for both practical surface combatant 5415 and basic surface-piercing truncated cylinder geometries. Towing tank experiments include PMM force and moment measurements and for the surface combatant TPIV for the bow region and preliminary 4D-PTV. LES simulations for subcritical Reynolds and Froude numbers are conducted for the cylinder. The sway amplitudes and frequencies are based on previous 5415 and single-phase cylinder studies. TPIV results show the major vortices dynamic onset and progression with alternating strengths and signs in time and trajectories in space. At phases  $0^\circ$  and  $90^\circ$ , the results exhibit similarity with static drift  $\beta=0$  (straight ahead) and  $10^\circ$ , respectively. At the intermediate phases, the measurements show transition between these two conditions and substantial vortex interactions and unsteady separation for dynamic maneuvering. Vortex core analysis using  $Q$  criteria of the sonar dome vortices shows sinusoidal oscillation with 1<sup>st</sup>-order harmonic amplitude decreasing with progression. The core trajectory is loop-shaped but exhibits rather complicated shape changes along the vortex progression. The cylinder results show similarities with single phase studies, but with substantial free surface effects. Drag and lift show increase with amplitude and frequency with phase jump at frequency ratio  $fr=1$  due to switch from 2P to 2S vortex shedding. Medium grid LES shows good agreement for force amplitudes, phases and FFT and phased averaged frequencies, which provides confidence in the flow field predictions, which are analyzed and compared with precursory straight-ahead experiments and LES; and single-phase controlled oscillation results. The 5415 results are being used by NATO AVT-253 for assessment of predictions methods and the cylinder results are being used for analysis of the physics of free surface boundary layer and wake/wave interactions and turbulence anisotropy; and for guidance for the analysis of the 5415 results. 4D-PTV for 5415 and finer LES grids for the cylinder are in progress.*

### 1.0 INTRODUCTION

Smooth-surface vortex separation onset and progression is a ubiquitous flow feature and critical limiting factor for the design and operation of sea and air vehicles. Improvements in modeling and simulation capability are required to meet increased performance requirements and standardization of maritime regulations. For small amplitude static and dynamic maneuvers, both systems-based and physics-based CFD simulation method predictions are satisfactory; however, for large amplitude motions both approaches have difficulties, as shown by the results of the SIMMAN 2008 and 2014 Workshops (Stern et al., 2011; Simonsen et al., 2017).

Under the auspices of the AVT-183 Reliable Prediction of Separated Flow Onset and Progression for Air and Sea Vehicles significant progress was made for improved physical understanding and prediction capabilities for three-dimensional steady separation (NATO STO, 2017). The sea facet focused on large amplitude static drift  $\beta$  maneuvers for which benchmark validation experimental studies were conducted for surface combatant 5415  $\beta=0, 10$  and  $20^\circ$  (Yoon et al., 2014), KVLCC2 (very large crude carrier)  $\beta=30^\circ$  (Abdel-Maksoud et al., 2015)



Figure 13 Schematics (left), PMM carriage (middle) and setup for surface piercing truncated cylinder (right)

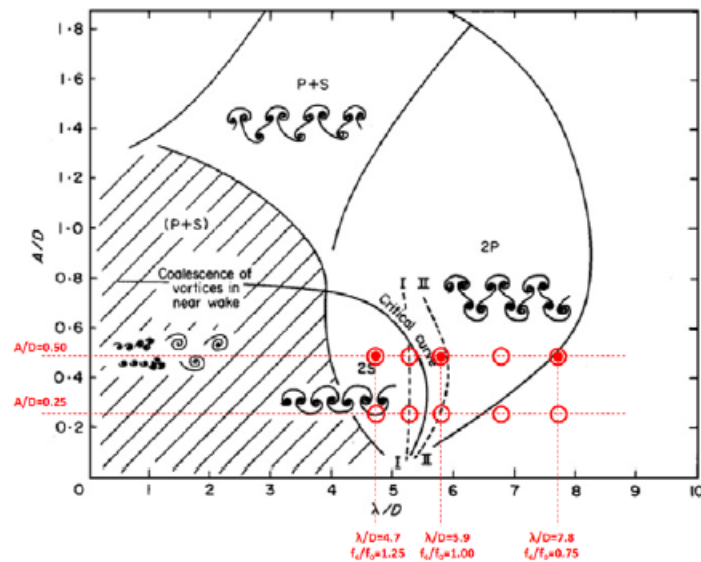


Figure 14 The map of regimes for vortex wake modes for controlled oscillating cylinder [Williamson and Roshko (1988), Williamson and Govardhan (2008)]; I, II are the curves where the forces on the body show a sharp "jump"; from Bishop and Hassan (1964). I is for wavelength decreasing and II is for wavelength increasing.

### Effects of Sway Motion on Smooth-Surface Vortex Separation Onset

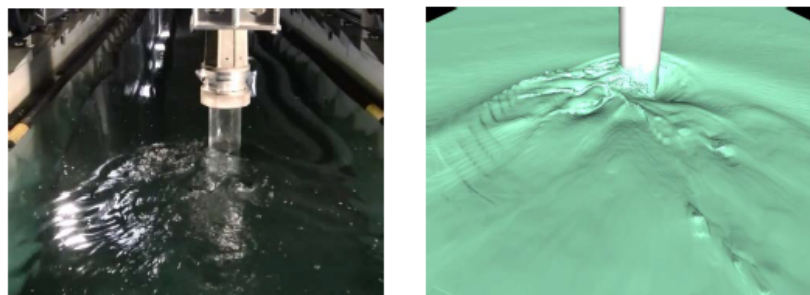


Figure 17 Photos of free surface waves around the cylinder and comparisons with the present LES simulations for  $(Re, Fr, AR, GR) = (123,000, 0.5, 4T, M)$  at  $y=y_{max}$ . ( $fr=1.25$ )

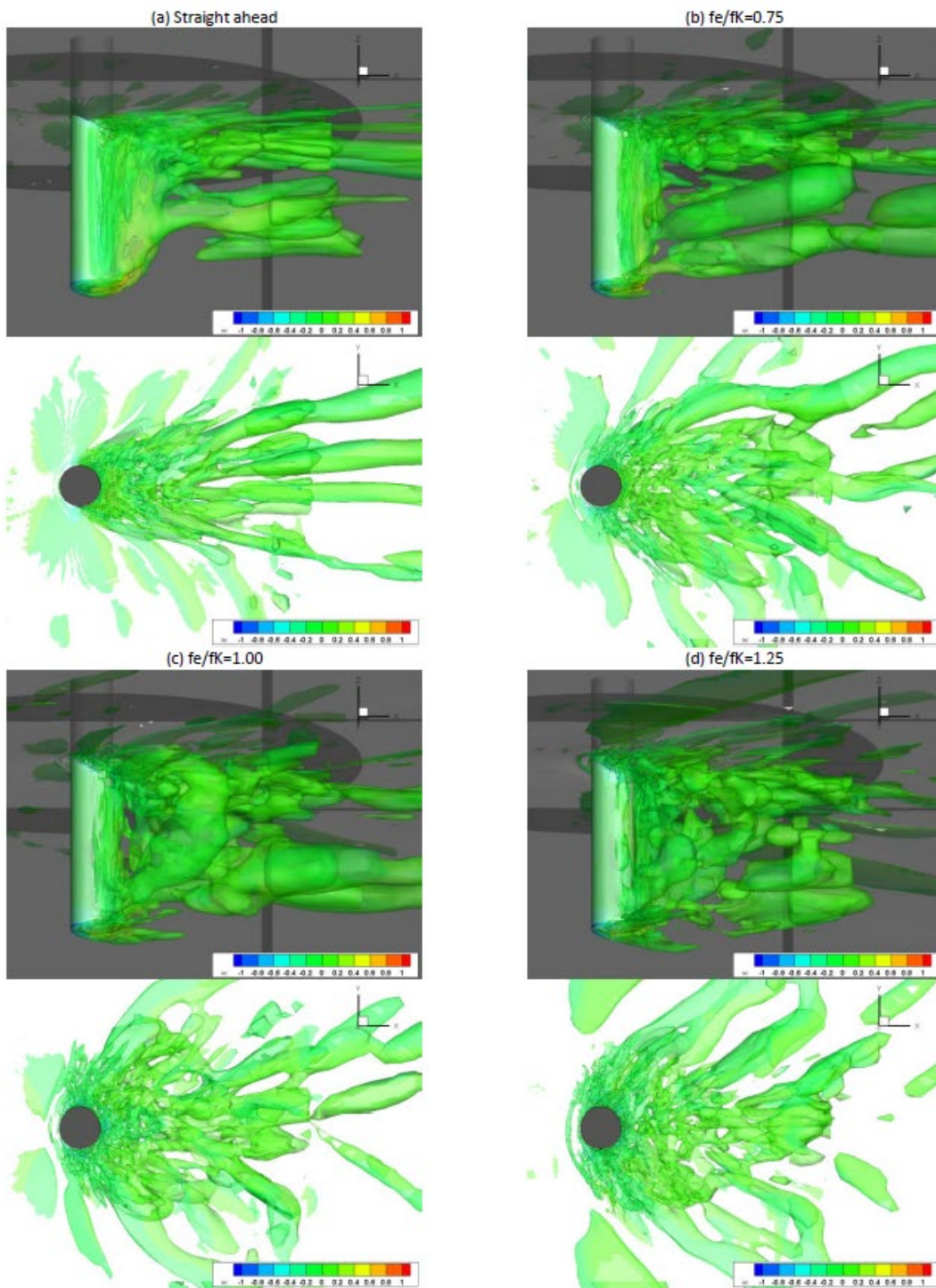


Figure 21 Iso-surface of mean Q-criterion ( $Q=0.04$ ) for  $(Re, Fr, AR, GR)=(123,000, 0.5, 4T, M)$ : (a) straight ahead, (b)  $fe/fK=0.75$ , (c)  $fe/fK=1.00$ , (d)  $fe/fK=1.25$